

# ParisLuco3D: A high-quality target dataset for domain generalization of LiDAR perception

Jules Sanchez<sup>1\*</sup>, Louis Soum-Fontez<sup>1\*</sup>, Jean-Emmanuel Deschaud<sup>1</sup>, and Francois Goulette<sup>1,2</sup>

**Abstract**—LiDAR is a sensor system that supports autonomous driving by gathering precise geometric information about the scene. Exploiting this information for perception is interesting as the amount of available data increases.

As the quantitative performance of various perception tasks has improved, the focus has shifted from source-to-source perception to domain adaptation and domain generalization for perception. These new goals require access to a large variety of domains for evaluation. Unfortunately, the various annotation strategies of data providers complicate the computation of cross-domain performance based on the available data

This paper provides a novel dataset, specifically designed for cross-domain evaluation to make it easier to evaluate the performance of various source datasets. Alongside the dataset, a flexible online benchmark is provided to ensure a fair comparison across methods.

## I. INTRODUCTION

LiDAR-based perception for autonomous driving applications has become increasingly popular in the last few years. LiDAR provides reliable and precise geometric information and is a useful addition to typical camera-based systems. The various LiDAR perception tasks have gained access to a growing number of open-source datasets, including semantic segmentation, object detection and tracking datasets. This large amount of data, and the thorough efforts of the community, have led to very good performance, notably by Cylinder3D [1] for LiDAR Semantic Segmentation (LSS) and PV-RCNN [2] for LiDAR Object Detection (LOD).

As a result, new tasks for evaluating the robustness of these methods in new scenarios and environments have emerged. Specifically, domain adaptation and domain generalization become the focus of LiDAR perception. These methods involve confronting a model trained on a specific domain with a new domain at the time of inference. In practice, a subset of datasets are used for training, and other datasets expected to be acquired elsewhere are used for testing.

While open-source datasets display a large variety of scenes and sensor setups, crucial discrepancies between labels sets have been identified ([3], [4]). Due to this label difference, it is not possible to leverage current online benchmarks to ensure fair comparisons across methods.

Some studies have worked around this issue by using synthetic datasets [5], to which any label set can be easily applied. We believe this workaround is insufficient, as

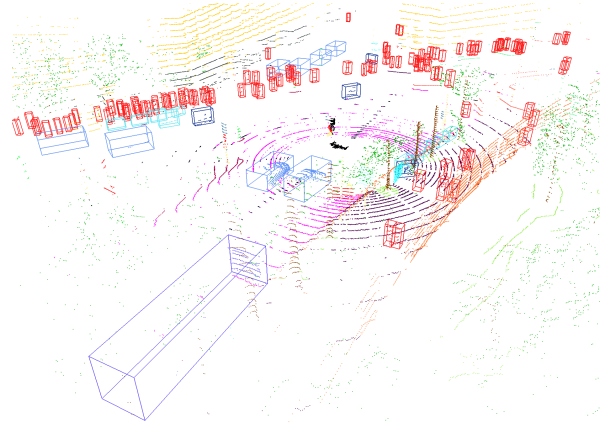


Fig. 1: An extract of the ParisLuco3D sequence.

synthetic datasets have proven to be very different from real datasets [6].

We propose here a new dataset, specifically designed for domain generalization evaluation, with annotations that can be easily mapped to existing standard datasets to avoid the need for comprise in quality evaluations of the domain generalization methods. As this dataset is focused on cross-domain evaluation, its annotations are not made available to the public.

This dataset was annotated by LiDAR perception experts over the course of 350 hours through a peer-reviewed process to ensure its quality. Our contributions are as follows:

- The release of a novel dataset, alongside an online benchmark, to compute cross-domain performances fairly. The choice of annotation allows this dataset to be used for various perception tasks: LSS, LOD, and tracking.
- A thorough overview of the generalization capabilities of current state-of-the-art architecture for both semantic segmentation and object detection in order to provide the community with a baseline for these tasks.

## II. RELATED WORK

### A. LiDAR Datasets in autonomous driving

The tasks that we are focusing on for perception are LSS, LOD and Tracking.

A summary of the main datasets along with the tasks they are annotated for, sensor information, and the amount of frames available, can be found in Table I.

The two most common perception tasks, measured by the amount of annotations available or the number of published

\*Equal contributions

<sup>1</sup>Centre for Robotics, Mines Paris - PSL, PSL University, 75006 Paris, France `firstname.surname@minesparis.psl.eu`

<sup>2</sup>U2IS, ENSTA Paris, Institut Polytechnique de Paris, 91120 Palaiseau, France `firstname.surname@ensta-paris.fr`

Name	Year	# scans train for LSS	# scans validation for LSS	LSS	LOD	Tracking	Location	Scene type	Sensor resolution (°)		# beams
									vertical	horizont.	
KITTI [7]	2012	N/A	N/A	×	~	×	Germany	suburban	0.4	0.08	64
SemanticKITTI [8]	2019	19k	4071	✓	×	✓	Germany	suburban	0.4	0.08	64
nuScenes [9]	2020	29k	6019	✓	✓	✓	US+Singapore	urban	1.33	0.32	32
SemanticPOSS [10]	2020	N/A	2988 <sup>†</sup>	✓	×	×	China	campus	0.33-6	0.2	40
Waymo [11]	2020	24k	5976	✓	✓	✓	US	urban	0.31	0.16	64
ONCE [12]	2021	N/A	N/A	×	✓	×	China	sub.+urban	0.33-6	0.2	40
Pandaset [13]	2021	N/A	6080 <sup>†</sup>	✓	✓	✓	US	suburban	0.17-5	0.2	64
HelixNet [14]	2022	49k	8179	✓	×	×	France	sub.+urban	0.4	0.08	64
KITTI-360 [15]	2023	60k	15204	~	✓	×	Germany	suburban	0.4	0.08	64
ParisLuco3D (Ours)	2023	N/A	7501 <sup>†</sup>	✓	✓	✓	France	urban	1.33	0.16	32

TABLE I: Summary of the various existing LiDAR perception datasets. <sup>†</sup>size of the full dataset as there is no designated split. KITTI provides LOD annotation only for a subset of the point cloud. KITTI-360 provides the LSS annotation on the accumulated and subsampled point cloud rather than on each scan (LSS = LiDAR Semantic Segmentation and LOD = LiDAR Object Detection).

works in these fields, are semantic segmentation and object detection. Accordingly, these tasks will be the focus of the remainder of this work.

#### 1) Datasets for LiDAR Semantic Segmentation (LSS):

The first dataset released for LSS was SemanticKITTI [8] in 2019, which was derived from the KITTI [7] dataset. It is acquired in a German suburb. Due to its size and seniority, it is the reference dataset for LiDAR semantic segmentation. Its annotations are evenly split between road users and background classes.

SemanticKITTI was then expanded into KITTI-360 [15], which includes data on the same suburb but on a much larger scale.

Later, some object detection datasets were expanded to incorporate semantic segmentation annotation, such as nuScenes [9] and Waymo [11]. They were acquired in cities and suburbs in the US and in Asia. Contrary to SemanticKITTI, nuScenes focuses its annotations on vehicles with a limited amount of background classes.

Recently, a few more large scale datasets have been released, such as HelixNet [14] and Navya-3Dseg [16], but due to their recency they have yet to be used in the LSS literature. They are acquired in French cities and suburbs.

Finally, some additional targeted datasets were released, such as SemanticPOSS [10], which proposed a new setup by providing a dataset acquired in a student campus, and Pandaset [13], which has a double-sensor setup.

Besides the variety of location of acquisition, in Table I we can observe the variety of sensor resolutions as well.

#### 2) Datasets for LiDAR Object Detection (LOD):

In 2014, KITTI [7] was released and ushered in a new range of experimental data for LOD. While there are several downsides in its annotation, such as the limited number of classes and the limited annotated field of view, it has remained an important benchmark for detection due to the quality of its annotations and its high-density point clouds.

The nuScenes [9] dataset was later released with full 360 degrees annotations, and an exhaustive list of annotated classes. Even though the number of available scans is higher than KITTI, due to the frequency of the sensor and its resolution, they are much sparser.

The Waymo [11] dataset is the one with the most 3D

annotations, along with a high number of high-density point clouds. Nevertheless, it only contains coarse class information, whereas other datasets have a finer label space. Its environment is also mostly restricted to urban American cities.

Finally, new datasets were released in an attempt to diversify the environments and LiDAR sensors used for detection, such as the ONCE [12] dataset. This dataset uses a 40-beam LiDAR sensor, resulting in an atypical point cloud density distribution. However, most of its data are left unlabeled for tasks like unsupervised learning.

#### B. Domain generalization for LiDAR perception

Domain generalization was long reserved for 2D perception [17], as domain adaptation was the main focus of 3D research. The difference between these fields is that domain generalization does not use any information before processing the new domain.

Recently, some works on domain generalization of LiDAR perception have emerged, especially for object detection [18] by adversarial augmentation, and for semantic segmentation [3], [19], [20], [21] using domain alignment by identifying a canonical representation either in the feature space or in the euclidean space. Furthermore, MDT3D [22] is focused on multi-source domain generalization.

They all highlight the difficulties of performing cross-domain evaluation, as annotations can and do differ from one dataset to another. Specifically, they have to resort to studying either the intersection of the label set [21], usually on very few labels, or a remapping to a common, coarser label set [3].

ParisLuco3D provides a new annotation set that can be mapped to any reference dataset, and cross-domain evaluation can be done fairly without any compromise regarding the fineness of the label set. Furthermore, while this dataset could be considered small, as it is only used for evaluation, it is on par or even bigger than most validation sets.

### III. DATASET PRESENTATION

#### A. Acquisition and Data generation

1) *Acquisition:* The acquisition of the ParisLuco3D dataset was carried out on November 17, 2015, over a

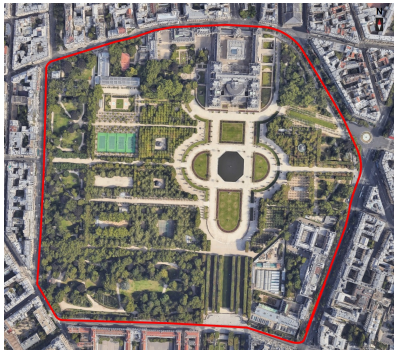


Fig. 2: Trajectory of our dataset (2.1 km around the Luxembourg Garden in Paris) overlaid on Google Satellite Image of Paris.



Fig. 3: Illustrations showing the diversity of scenes and quality of annotation in the ParisLuco3D dataset (left: point clouds by accumulating the scans of our dataset colorized with labels<sup>1</sup>; right: images taken from Google Street View).

distance of 2.1 km, in 12 min, at an average speed of 7.2 km/h. The trajectory, shown in Figure 2, is around the Luxembourg Garden in the heart of the city of Paris. Figure 3 shows point clouds by accumulating the scans and illustrate the diversity of scenes and contexts in our dataset.

The LiDAR used was a Velodyne HDL32 positioned vertically on a pole itself attached to the roof of a Citroën Jumper vehicle. Due to its placement and size of the vehicle, the sensor was about 3.70 m from the ground (a height different than what is usually available in other LiDAR datasets in autonomous driving).

The weather changed during the acquisition, with rain arriving in the middle of the acquisition. This has a visible impact in the LiDAR data with, for example, pedestrians carrying open umbrellas (which significantly changes their representation) or certain parts of the road that could not be captured due to flasks of water.

<sup>1</sup>Pedestrians and road users have been removed from some point clouds for better viewing

2) *Data generation*: The ParisLuco3D dataset consists of 7501 scans in the form of 3D point clouds (a scan is a 360-degree horizontal rotation of the LiDAR sensor). The data are available in raw format with the following information:  $x$ ,  $y$ ,  $z$ ,  $timestamp$ ,  $intensity$ ,  $laser\_index$ .

*Intensity* is the intensity of the return signal, which represents 256 calibrated reflectivity values (diffuse reflectors are represented with values ranging from 0–100 and retro-reflectors from 101–255)<sup>2</sup>.

*Timestamp* is the time per point provided by the LiDAR sensor, synchronized with a GPS sensor. The *laser\_index* refers to the number of the laser that fired (32 lasers in the Velodyne HDL32). Finally, *timestamp* and *laser\_index*, which are often not available in other datasets [8], [9], [11], [10], [13], can allow the development of specific methods, such as the Helix4D [14], which exploits the timestamp.

This raw data do not take into account the movement of the vehicle during a scan. To estimate this movement, we used CT-ICP [23] LiDAR odometry, which enables calculating the deformation of the scans. We therefore also provide motion-corrected scans with the same information as raw scans:  $x$ ,  $y$ ,  $z$ ,  $timestamp$ ,  $intensity$  and  $laser\_index$ . All data annotations (semantic class per points, bounding boxes of objects) were made on these motion-corrected scans.

Finally, to allow methods using data sequentiality (i.e. past scans), we also used CT-ICP to compute a pose for each scan (motion-corrected) in a world frame corresponding to the frame of the first scan of the sequence. The poses are provided in KITTI format [7] and correspond precisely to the pose of the vehicle in the middle of a scan acquisition (i.e. when the LiDAR lasers fire forward like the KITTI convention).

The sequence is composed of a loop, with an overlap of about 150 m between the start and end of the acquisition. A registration by ICP [24] on the overlap zone and a graph SLAM solver [25] allowed us to calculate the final poses with loop closure.

## B. Label shift & Annotation process

1) *Label shift*: A major issue when conducting cross-dataset evaluation is the difference in label set definitions. There are three sources of differences, which we illustrate for the semantic segmentation case.

First, some objects are annotated in one dataset but not in another. An example of this is the "traffic cone" annotation found in nuScenes but not in SemanticKITTI.

Second, there are granularity differences. For example, nuScenes defines "manmade", whereas SemanticKITTI distinguishes "building", "pole", "sign". Similarly, Waymo uses a single *Vehicle* class instead of separating between cars, trucks or buses.

Finally, there is something we call the *label shift* which represents different objects under similar labels. An example of label shift is the definitions of "road" and "sidewalk" in nuScenes and SemanticKITTI. In one dataset, bike lanes are

<sup>2</sup><https://tinyurl.com/ycxm2d7a>

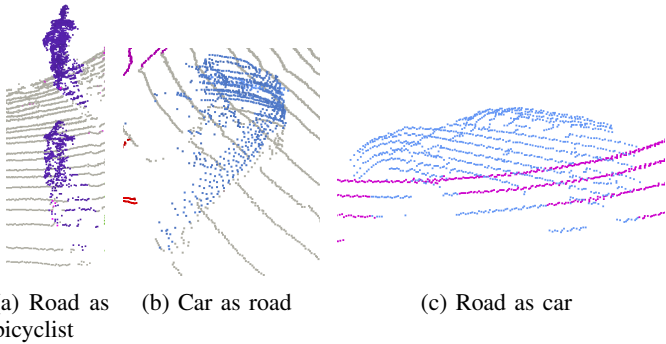


Fig. 4: Some common annotations mistakes in SemanticKITTI (a),(b) or in SemanticPOSS (c).

part of the "road" label, whereas in the other dataset they part of the "sidewalk" label.

Similar issues appear for 3D object detection. For instance, we observe a granularity difference between Waymo and nuScenes, going from 3 classes to 10.

Furthermore, *label shift* appears and results in change for bounding box dimensions. For instance, the Waymo dataset does not include large objects carried by pedestrians in its bounding boxes and does not annotate any parked bicycles.

2) *Annotation process*: In order to guarantee the quality of the annotations in this dataset, we relied on expert annotators working in the field of 3D point cloud processing for years who have experience working with existing datasets. The dataset was triple-checked in order to catch any mistakes.

Some examples of annotation mistakes occurring in reference datasets can be seen in Figure 4.

The software used for the semantic segmentation annotation is *point labeler* [8], while the one for object detection is *labelCloud* [26], which are both open-source.

### C. Labels for semantic segmentation

Dataset	# labels	# labels $\cap$ SK	# labels $\cap$ NS	# labels $\cap$ PL
SemanticKITTI [8]	19	N/A	10	19
nuScenes [9]	16	10	N/A	16
Pandaset [13]	37	8	8	13
Waymo [11]	22	15	11	20
KITTI-360 [15]	18	15	13	16
SemanticPOSS [10]	13	11	6	13
HelixNet [14]	9	7	6	7
ParisLuco3D	45	19	16	N/A

TABLE II: Number of labels of each LSS dataset and the size of the intersection of their label set with SemanticKITTI's (SK) and nuScenes' (NS).

In Table II, we summarize the number of labels from the various datasets and how many of these labels are intersecting with the label sets of nuScenes and SemanticKITTI. We chose these two datasets because they are the commonly used training sets. We see, when cross-domain evaluation is conducted, a significant drop in the number of labels for evaluation and a loss of fineness for prediction.

For ParisLuco3D, we wanted to define a label set that could be easily mapped to nuScenes and SemanticKITTI, as

they are the two reference training sets. As such, annotation details of nuScenes and SemanticKITTI were dissected to understand which objects is encapsulated in each label to avoid a label shift between ParisLuco3D and these datasets. It results in fine annotation, avoiding any ambiguity in the remapping.

There are 45 labels for semantic segmentation: car, bicycle, bicyclist, bus, motorcycle, motorcyclist, scooter, truck, construction-vehicle, trailer, person, road, bus-lane, bike-lane, parking, road-marking, zebra-crosswalk, roundabout, sidewalk, central-median, building, fence, pole, traffic-sign, bus-stop, traffic-light, light-pole, bike-rack, parking-entrance, metro-entrance, vegetation, trunk, vegetation-fence, terrain, temporary-barrier, pedestrian-post, garbage-can, garbage-container, bike-post, bench, ad-spot, restaurant-terrace, road-post, traffic-cone, and other-object.

These labels cover the usual autonomous driving labels as well as the more specific features of specific case of the Paris landscape, such as metro entrances or bar terraces. The mapping details for recovering the label sets of SemanticKITTI and nuScenes can be found in the supplementary material.

Due to the nature of the scene, we observe a large quantity of pedestrians and buses. The details of the label distribution are presented in Figure 5. Examples of every label can be found in the supplementary material.

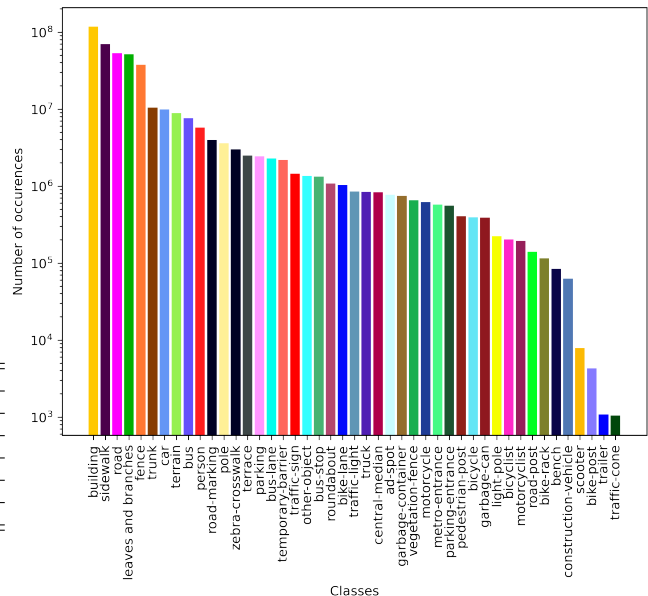


Fig. 5: Distribution of the labels in ParisLuco3D.

### D. Labels for object detection

Similarly to most autonomous driving datasets, we mainly focused on road agents and cover them all with our 11 labels. These are car, bus, truck, trailer, bicycle, bicyclist, motorcycle, motorcyclist, scooter, scootercyclist, and pedestrian.

We took into account the specificities of the common classes between datasets when choosing our labels and the level of granularity to ease the mapping when working in

a cross-dataset setting, which we believe to be relevant for the generalization task. We also seek to be as fine-grained as possible for road users, and base our fine-grained LOD classes on the nuScenes dataset, which are easily mappable on the other datasets, specifically ONCE and Waymo. The specific mappings can be found in the supplementary.

Whenever possible, we also distinguish between static objects and dynamic ones, such as *bicycle* and *bicyclist*. We also provide examples of every type of labelled object in the supplementary materials. Due to the high redundancy between LiDAR scans, we only annotated one out of ten frames with bounding box annotations, which we call *keyframes*. Non-keyframes scans were also used to help guide the annotation process. As shown in Table III, we have the highest number of pedestrians per annotated LiDAR scan compared to other datasets, which are notoriously difficult to detect at long ranges.

Name	Classes	3D Boxes	instances per scan		
			car	bicycle	pedestrian
KITTI [7]	3	18k	3.8	0.2	0.6
nuScenes[9]	23/10*	149k	11	0.3	5.7
Waymo [11]	3	1.8M	29.8	0.3	13.5
ONCE [12]	5	90k	19.8	6.3	2.9
ParisLuco3D	11	64k	14.7	6.4	56.3

TABLE III: Comparison between 3D Object Detection datasets. All values are computed for the validation splits of the datasets. \*The 23 original classes of nuScenes are generally grouped into 10 due to a strong similarity in some fine classes, for instance *standing pedestrians* and *sitting pedestrians*.

Due to the natural occlusion phenomenon that occurs during traversal of the environment, some annotated objects may not contain any points. However, if during the annotation process we were aware of the presence of an object, by aggregating sequential point clouds for instance, we maintained its annotation in order to facilitate both annotation and the tracking task.

While we annotated bounding boxes to their maximum range, certain filters are applied while evaluating them to ensure a fair evaluation process. First, only boxes whose center was within 50 m of the sensor were kept. Second, since many boxes were kept between keyframes even if they did not contain any points, we would not expect any model to predict them. In practice, we filter out boxes that contain 5 points or less.

For a given 3D *keyframe* scan containing  $N$  annotated objects, bounding box annotations are represented as follows:

$$\{b_i = (cx_i, cy_i, cz_i, l_i, w_i, h_i, \theta_i)\}_{i \in [1, N]}$$

where  $cx_i, cy_i$ , and  $cz_i$  represent the center of the bounding box annotation along the  $x, y$  and  $z$  coordinates,  $l_i, w_i$  and  $h_i$  represent the length, width and height, and  $\theta_i$  represents the heading of the bounding box.

### E. Labels for Tracking

Every element inside the object detection annotations was tracked. This means that there are also 11 classes for

tracking, and one of out 10 frames were annotated.

While detection computes scores for boxes populated with more than 5 points, objects that are dropping below 5 points due to occlusion are still tracked.

## IV. OVERVIEW OF LiDAR DOMAIN GENERALIZATION ON PARISLUCO3D

To illustrate the importance of providing a new dataset specifically targeting domain generalization, in the following section we benchmark current state-of-the-art methods of semantic segmentation and object detection, using ParisLuco3D as the target dataset to avoid the need to compromise on the label set at the time of evaluation.

### A. LiDAR semantic segmentation

1) *Related work*: LSS builds upon the typical 2D convolutional neural networks. Earlier approaches projected the 3D point cloud into a 2D representation, either with a range projection [27] or with a bird’s-eye-view (BEV) projection [28]. While these methods were extremely fast, their performance was not satisfactory

In parallel, point-based architectures were developed, either based on order-agnostic operation [29] or by taking the time to redefine the convolution [30].

The highest performing methods are the sparse voxel-based [31] models, which restructure the point cloud into a regular 3D grid and apply 3D convolution to it [32], [1].

Recently, some methods have started to exploit the acquisition pattern of typical LiDAR sensors to achieve a high inference speed with a limited decrease in performance [14].

2) *Experiments*: To compute domain generalization performance, two datasets are required. One is used as the training set, called case the source set, while the other is used as the test set, called the target set. The target set is supposed to have never been seen at any point in the training process. As source sets, we used two datasets considered to be standard: nuScenes and SemanticKITTI. They are considered standard due to their size and seniority.

The target set is ParisLuco3D. The details of the mapping from the original label set to the SemanticKITTI and nuScenes label sets can be found in the supplementary material.

Model	Input type	$SK \rightarrow PL^*$		$NS \rightarrow PL$	
		mIoU <sub>SK</sub>	mIoU <sub>PL</sub>	mIoU <sub>NS</sub>	mIoU <sub>PL</sub>
CENet [27]	Range	58.8	21.6	69.1	31.6
PolarSeg [28]	BEV	61.8	9.6	71.4	11.3
KPCov [30]	Point	61.8	20.3	64.2	22.9
SRUNet [31]	Voxel	63.2	<b>30.7</b>	69.3	37.4
SPVCNN [32]	Point+Voxel	63.4	28.9	66.8	<b>38.7</b>
Helix4D [14]	4D Point	63.9	18.3	69.3	19.2
Cylinder3D [1]	Cyl. voxel	<b>64.9</b>	23.0	<b>74.8</b>	25.5

TABLE IV: Generalization baseline when trained on SemanticKITTI (SK), or nuScenes (NS), and evaluated on ParisLuco3D (PL). \*When SemanticKITTI is the source, the reflectivity channel is not used.

We computed the generalization results for seven different neural architectures from SemanticKITTI to ParisLuco3D

and for five architectures from nuScenes to ParisLuco3D (Table IV). This difference in the number of models tested is due to the unavailability of some of them with nuScenes as a source set.

All methods were trained with the respective original sets of SemanticKITTI and nuScenes, and evaluated on it.

These different models were selected due to their representativeness of the various input types (projection-based, point-based, voxel-based), the availability of the source code and of the pre-trained weights, and the quality of their source-to-source results.

To date, very few semantic segmentation domain generalization methods for LiDAR point clouds were released. The most notable one [3] has not made its code available, and thus we did not benchmark it.

The metric used for the computation of the semantic segmentation performance is the Intersection over Union (IoU) for each class, and its mean (mIoU). Introducing TP (True Positive), FP (False Positive), and FN (False Negative), the IoU can be written as follows:

$$IoU = \frac{target \cap prediction}{target \cup prediction} = \frac{TP}{TP + FP + FN} \quad (1)$$

It is measured up to 50 meters away to the sensor, similarly to SemanticKITTI.

3) *Results & analysis*: The per-class results can be found in the supplementary material.

For SemanticKITTI to ParisLuco3D, all architectures were retrained without the reflectivity channel. As the sensors used in the two datasets varied, the reflectivity decreased the generalization performance. In Table V, we illustrate this decrease in performance in several cases. Overall, the results in Table IV and Table V are unsatisfying, especially for the pedestrian class (see the supplementary material) which is critical for autonomous driving applications.

For nuScenes to ParisLuco3D, the results were computed with the reflectivity channel, as the same sensor is used in both datasets. This is also illustrated in Table V. The results were much better in this case, the low mIoU comes from the trailer and traffic cone categories for which there are very few examples in ParisLuco3D.

Model	<i>SK</i> → <i>PL</i>		<i>NS</i> → <i>PL</i>	
	mIoU <sub>SK</sub>	mIoU <sub>PL</sub>	mIoU <sub>NS</sub>	mIoU <sub>PL</sub>
SRUNet [31] with reflectivity	66.6	27.9	69.3	37.4
SRUNet [31] without reflectivity	63.2	30.7	66.3	32.3
Cylinder3D [1] with reflectivity	70.4	2.7	74.8	25.5
Cylinder3D [1] without reflectivity	64.9	23.0	70.2	17.1

TABLE V: Impact of the reflectivity channel on some architectures on their generalization performance.

Table IV shows that the best performing generalization methods were the voxel-based one, except for Cylinder3D due to its intra-voxel PointNet feature extractor.

## B. LiDAR Object Detection

1) *Related work*: LOD is generally done by using features extracted by subdividing the 3D space in voxels and applying local shape feature extractors such as PointNet [29], which are then followed by convolutional filters following the same methods as 2D neural network-based Object Detection. Works such as SECOND [33] and PointPillars [34] sought to increase the speed of using these convolutions to enable real-time applications.

However, point-based methods also exist. For instance, PointRCNN [35] obtains multi-range features by subdividing input point clouds into three according to their distance and computing their local features, which are then used to optimize bounding box predictions.

The most performing methods typically use two-steps processes of initial proposals and refinement using features interpolated from keypoints [2], [36]. Recently, methods have been exploring predictions based on object centers [37] as well as transformer-based architectures [38].

2) *Experiments*: We established a benchmark for testing models on our ParisLuco3D dataset. As we aimed to test the domain generalization performance of detection models, we trained them on source datasets, ONCE and Waymo, and then evaluated them on ParisLuco, using the latter as a test set. Therefore, ParisLuco scans and annotations were not used during the training process. We chose ONCE and Waymo due to both their size and their differences in LiDAR sensors, respectively a 40-beam sensor for ONCE and a 64-beam LiDAR sensors for Waymo. We used our label mapping, detailed in the supplementary materials, to enable the transfer of models trained on a set of labels to our new labels.

We evaluated the generalization ability of five different 3D object detection models across the various choices of source datasets: SECOND [33], PointRCNN [35], PointPillars [34], PV-RCNN [2], and CenterPoint [36]. These models were chosen due to their availability and their performance across different 3D object detection benchmarks.

We also implement some traditional methods used for domain generalization, namely instance normalization similarly to the implementation of IBN-Net [39] for semantic segmentation, and ray-dropping data augmentations, where we dropped between 25% and 60% of LiDAR beams at the time of training to emulate lower-resolution sensors, inspired by Theodose et al. [40].

The predictions were evaluated by considering those with low overlap with ground-truth bounding boxes as false positives. We used IoU thresholds specific to each class for this, specifically 0.7 for four-wheel vehicles, 0.5 for two-wheel vehicles, and 0.3 for pedestrians. Furthermore, we use the average precision (AP) metric, which is commonly used for the 3D object detection task, and its mean across all classes (mAP). The average precision for a given class is defined as the precision integrated over a fixed range of recall values. We chose 50 recall values ranging between 0.02 and 1, following the protocol of ONCE:

## V. ONLINE BENCHMARK

$$AP = \frac{1}{50} \sum_{r=1}^{50} p\left(\frac{1}{r}\right), \quad p = \frac{TP}{TP+FP} \quad (2)$$

Model	ON $\rightarrow$ PL		W $\rightarrow$ PL	
	mAP <sub>ON</sub>	mAP <sub>PL</sub>	mAP <sub>W</sub>	mAP <sub>PL</sub>
PointRCNN [35]	28.6	8.3	47.9	16.2
PointPillars [34]	45.5	<b>12.4</b>	68.1	<b>30.2</b>
PV-RCNN [2]	52.4	10.6	72.3	22.8
SECOND [33]	54.0	9.9	69.5	23.0
CenterPoint [36]	<b>59.5</b>	8.5	<b>77.6</b>	25.3
PV-RCNN [2] +RayDrop [40]	48.3	17.1	N/A	N/A
PV-RCNN [2] +IBN-Net [39]	47.0	17.0	N/A	N/A

TABLE VI: Generalization baseline for 3D object detection when trained on ONCE (ON), or Waymo (W) and evaluated on ParisLuco3D (PL). The reflectivity channel is not used.

3) *Results & analysis:* We present our benchmark results in Table VI in terms of mAP, while individual per-class AP metrics are available in the supplementary material. Our models were trained without the reflectivity channel (we underlined in Table V how reflectivity hinders models’ generalization abilities for semantic segmentation). We also show this in Table VII for object detection. We trained a SECOND model on the nuScenes dataset both with and without reflectivity and found that reflectivity improved performance in the case in which the LiDAR sensor is the same to the one used for training.

Model	ON $\rightarrow$ PL		NS $\rightarrow$ PL	
	mAP <sub>ON</sub>	mAP <sub>PL</sub>	mAP <sub>NS</sub>	mAP <sub>PL</sub>
SECOND [33] with reflectivity	54.1	7.1	45.9	8.9
SECOND [33] without reflectivity	54.0	9.9	42.1	8.0

TABLE VII: Impact of the reflectivity channel on generalization performance for the detection task.

In Table VI, we see that despite its relatively low source mAP, the PointPillars models tends to generalize better on ParisLuco3D when trained on ONCE or Waymo. We believe that there are two reasons for this. First, it contains a lower number of parameters, and so it tends to be less susceptible to overfitting. Furthermore, its mAP is highly elevated by its accuracy in the *Pedestrian* class (see the supplementary material) due to the high priors in the model in the form of its reliance on anchors, which are sensitive to dimension changes, which are quite rare for pedestrians. Both RayDrop and IBN-Net increase the generalization of the PV-RCNN model, but our RayDrop augmentation tends to increase AP for the *Pedestrian* class, which could be the result of the low average number of points on the surface of these class instances in our urban environment.

Overall, we found that even with some simple domain generalization methods, both LOD and LSS models suffer from large accuracy drops when transferred to our ParisLuco3D dataset, highlighting the need for novel methods.

To ensure a fair measurement of the domain generalization performance on this dataset, the ground-truth labels will not be released but only the raw dataset. For qualitative comparisons of methods, five scans will be released alongside their annotations. They can be found in the supplementary material.

Nonetheless, to provide the community with a tool beyond the dataset itself, we establish an online benchmark to test the domain generalization and unsupervised domain adaptation methods.

The online benchmark will be put in place for three LiDAR perception tasks: semantic segmentation, object detection and object tracking.

For semantic segmentation and object detection, two setups will respectively be possible. For LSS, 17 and 16 labels to match SemanticKITTI and nuScenes label sets will be available. For LOD, 10 and 5 labels to match nuScenes and ONCE will be available.

For tracking, the benchmark will align with nuScenes, and thus will be ranked according to the AMOTA (Average Multi Object Tracking Accuracy), with the classes defined for object detection.

Two different benchmarks will be accessible, one on the website of the dataset, reserved for published methods, and one on CodaLab<sup>3</sup>, where anyone will be welcome to participate. We encourage authors to avoid typical benchmark optimization techniques in order to fairly judge generalization performance. Following [41], the number of submission will be limited.

## VI. CONCLUSION

In this paper, we proposed a new dataset for LiDAR perception. This dataset stands out from the already released dataset due to the fineness of the annotations, the relatively unexplored setup of dense urban european cities, and its goal of domain generalization.

We hope that this dataset will enable to see in our community the emergence of new 3D perception methods that generalize well.

## ACKNOWLEDGMENT

We would like to thank Hassan Bouchiba who mainly contributed to the acquisition of this dataset back in 2015.

## REFERENCES

- [1] X. Zhu, H. Zhou, T. Wang, F. Hong, Y. Ma, W. Li, H. Li, and D. Lin, “Cylindrical and asymmetrical 3d convolution networks for lidar segmentation,” in *2021 IEEE/CVF Conference on Computer Vision and Pattern Recognition (CVPR)*, 2021, pp. 9934–9943.
- [2] S. Shi, C. Guo, L. Jiang, Z. Wang, J. Shi, X. Wang, and H. Li, “Pv-rcnn: Point-voxel feature set abstraction for 3d object detection,” in *2020 IEEE/CVF Conference on Computer Vision and Pattern Recognition (CVPR)*, 2020, pp. 10526–10535.
- [3] H. Kim, Y. Kang, C. Oh, and K.-J. Yoon, “Single domain generalization for lidar semantic segmentation,” in *Proceedings of the IEEE/CVF Conference on Computer Vision and Pattern Recognition (CVPR)*, June 2023, pp. 17587–17598.

<sup>3</sup>see <https://competitions.codalab.org/> for more information

- [4] J. Sanchez, J.-E. Deschaud, and F. Goulette, "Cola: Coarse label pre-training for 3d semantic segmentation of sparse lidar datasets," in *2023 IEEE International Conference on Robotics and Automation (ICRA)*, 2023, pp. 11 343–11 350.
- [5] C. Saltori, F. Galasso, G. Fiameni, N. Sebe, E. Ricci, and F. Poiesi, "Cosmix: Compositional semantic mix for domain adaptation in 3d lidar segmentation," in *Computer Vision – ECCV 2022*, S. Avidan, G. Brostow, M. Cissé, G. M. Farinella, and T. Hassner, Eds. Cham: Springer Nature Switzerland, 2022, pp. 586–602.
- [6] B. Wu, X. Zhou, S. Zhao, X. Yue, and K. Keutzer, "Squeezesegv2: Improved model structure and unsupervised domain adaptation for road-object segmentation from a lidar point cloud," in *2019 International Conference on Robotics and Automation (ICRA)*, 2019, pp. 4376–4382.
- [7] A. Geiger, P. Lenz, and R. Urtasun, "Are we ready for autonomous driving? the kitti vision benchmark suite," in *2012 IEEE Conference on Computer Vision and Pattern Recognition*, 2012, pp. 3354–3361.
- [8] J. Behley, M. Garbade, A. Milioto, J. Quenzel, S. Behnke, C. Stachniss, and J. Gall, "Semantickitti: A dataset for semantic scene understanding of lidar sequences," in *2019 IEEE/CVF International Conference on Computer Vision (ICCV)*, 2019, pp. 9296–9306.
- [9] H. Caesar, V. Bankiti, A. H. Lang, S. Vora, V. E. Liong, Q. Xu, A. Krishnan, Y. Pan, G. Baldan, and O. Beijbom, "nuscenes: A multimodal dataset for autonomous driving," in *2020 IEEE/CVF Conference on Computer Vision and Pattern Recognition (CVPR)*, 2020, pp. 11 618–11 628.
- [10] Y. Pan, B. Gao, J. Mei, S. Geng, C. Li, and H. Zhao, "Semanticpos: A point cloud dataset with large quantity of dynamic instances," in *2020 IEEE Intelligent Vehicles Symposium (IV)*, 2020, pp. 687–693.
- [11] P. Sun, H. Kretzschmar, X. Dotiwalla, A. Chouard, V. Patnaik, P. Tsui, J. Guo, Y. Zhou, Y. Chai, B. Caine, V. Vasudevan, W. Han, J. Ngiam, H. Zhao, A. Timofeev, S. Ettinger, M. Krivokon, A. Gao, A. Joshi, Y. Zhang, J. Shlens, Z. Chen, and D. Anguelov, "Scalability in perception for autonomous driving: Waymo open dataset," in *2020 IEEE/CVF Conference on Computer Vision and Pattern Recognition (CVPR)*, 2020, pp. 2443–2451.
- [12] J. Mao, M. Niu, C. Jiang, H. Liang, X. Liang, Y. Li, C. Ye, W. Zhang, Z. Li, J. Yu, et al., "One million scenes for autonomous driving: Once dataset," *NeurIPS*, 2021.
- [13] P. Xiao, Z. Shao, S. Hao, Z. Zhang, X. Chai, J. Jiao, Z. Li, J. Wu, K. Sun, K. Jiang, Y. Wang, and D. Yang, "Pandaset: Advanced sensor suite dataset for autonomous driving," in *2021 IEEE International Intelligent Transportation Systems Conference (ITSC)*, 2021, pp. 3095–3101.
- [14] R. Loiseau, M. Aubry, and L. Landrieu, "Online segmentation of lidar sequences: Dataset and algorithm," in *Computer Vision – ECCV 2022*, S. Avidan, G. Brostow, M. Cissé, G. M. Farinella, and T. Hassner, Eds. Cham: Springer Nature Switzerland, 2022, pp. 301–317.
- [15] Y. Liao, J. Xie, and A. Geiger, "Kitti-360: A novel dataset and benchmarks for urban scene understanding in 2d and 3d," *IEEE Transactions on Pattern Analysis and Machine Intelligence*, vol. 45, no. 3, pp. 3292–3310, 2023.
- [16] A. Almin, L. Lemarié, A. Duong, and B. R. Kiran, "Navya3dseg - navya 3d semantic segmentation dataset design & split generation for autonomous vehicles," *IEEE Robotics and Automation Letters*, vol. 8, no. 9, pp. 5584–5591, 2023.
- [17] K. Zhou, Z. Liu, Y. Qiao, T. Xiang, and C. C. Loy, "Domain generalization: A survey," *IEEE Transactions on Pattern Analysis and Machine Intelligence*, vol. 45, no. 4, pp. 4396–4415, 2023.
- [18] A. Lehner, S. Gasperini, A. Marcos-Ramiro, M. Schmidt, M.-A. N. Mahani, N. Navab, B. Busab, and F. Tombari, "3d-vfield: Adversarial augmentation of point clouds for domain generalization in 3d object detection," in *2022 IEEE/CVF Conference on Computer Vision and Pattern Recognition (CVPR)*, 2022, pp. 17 274–17 283.
- [19] C. Saltori, A. Ošep, E. Ricci, and L. Leal-Taixé, "Walking Your LiDOG: A Journey Through Multiple Domains for LiDAR Semantic Segmentation," *arXiv e-prints*, p. arXiv:2304.11705, 2023.
- [20] J. Sanchez, J.-E. Deschaud, and F. Goulette, "Domain generalization of 3d semantic segmentation in autonomous driving," in *Proceedings of the IEEE/CVF International Conference on Computer Vision (ICCV)*, October 2023, pp. 18 077–18 087.
- [21] L. Yi, B. Gong, and T. Funkhouser, "Complete & label: A domain adaptation approach to semantic segmentation of lidar point clouds," in *2021 IEEE/CVF Conference on Computer Vision and Pattern Recognition (CVPR)*, 2021, pp. 15 358–15 368.
- [22] L. Soum-Fontez, J.-E. Deschaud, and F. Goulette, "MDT3D: Multi-Dataset Training for LiDAR 3D Object Detection Generalization," *arXiv e-prints*, p. arXiv:2308.01000, 2023.
- [23] P. Dellenbach, J.-E. Deschaud, B. Jacquet, and F. Goulette, "Ct-icp: Real-time elastic lidar odometry with loop closure," in *2022 International Conference on Robotics and Automation (ICRA)*, 2022, pp. 5580–5586.
- [24] P. Besl and N. D. McKay, "A method for registration of 3-d shapes," *IEEE Transactions on Pattern Analysis and Machine Intelligence*, vol. 14, no. 2, pp. 239–256, 1992.
- [25] G. Grisetti, R. Kümmerle, C. Stachniss, and W. Burgard, "A tutorial on graph-based slam," *IEEE Intelligent Transportation Systems Magazine*, vol. 2, no. 4, pp. 31–43, 2010.
- [26] C. Sager, P. Zschech, and N. Kuhl, "labelCloud: A lightweight labeling tool for domain-agnostic 3d object detection in point clouds," *Computer-Aided Design and Applications*, vol. 19, no. 6, pp. 1191–1206, mar 2022. [Online]. Available: [http://cad-journal.net/files/vol.19/CAD.19\(6\).2022.1191-1206.pdf](http://cad-journal.net/files/vol.19/CAD.19(6).2022.1191-1206.pdf)
- [27] H. Cheng, X. Han, and G. Xiao, "Cenet: Toward concise and efficient lidar semantic segmentation for autonomous driving," in *2022 IEEE International Conference on Multimedia and Expo (ICME)*, 2022, pp. 01–06.
- [28] Y. Zhang, Z. Zhou, P. David, X. Yue, Z. Xi, B. Gong, and H. Foroosh, "Polarnet: An improved grid representation for online lidar point clouds semantic segmentation," in *2020 IEEE/CVF Conference on Computer Vision and Pattern Recognition (CVPR)*, 2020, pp. 9598–9607.
- [29] C. R. Qi, L. Yi, H. Su, and L. J. Guibas, "Pointnet++: Deep hierarchical feature learning on point sets in a metric space," in *Proceedings of the 31st International Conference on Neural Information Processing Systems*, ser. NIPS'17. Red Hook, NY, USA: Curran Associates Inc., 2017, p. 5105–5114.
- [30] H. Thomas, C. R. Qi, J.-E. Deschaud, B. Marcotegui, F. Goulette, and L. Guibas, "Kpconv: Flexible and deformable convolution for point clouds," in *2019 IEEE/CVF International Conference on Computer Vision (ICCV)*, 2019, pp. 6410–6419.
- [31] C. Choy, J. Gwak, and S. Savarese, "4d spatio-temporal convnets: Minkowski convolutional neural networks," in *2019 IEEE/CVF Conference on Computer Vision and Pattern Recognition (CVPR)*, 2019, pp. 3070–3079.
- [32] H. Tang, Z. Liu, S. Zhao, Y. Lin, J. Lin, H. Wang, and S. Han, "Searching efficient 3d architectures with sparse point-voxel convolution," in *Computer Vision – ECCV 2020*, A. Vedaldi, H. Bischof, T. Brox, and J.-M. Frahm, Eds. Cham: Springer International Publishing, 2020, pp. 685–702.
- [33] Y. Yan, Y. Mao, and B. Li, "Second: Sparsely embedded convolutional detection," *Sensors*, vol. 18, no. 10, 2018. [Online]. Available: <https://www.mdpi.com/1424-8220/18/10/3337>
- [34] A. H. Lang, S. Vora, H. Caesar, L. Zhou, J. Yang, and O. Beijbom, "Pointpillars: Fast encoders for object detection from point clouds," in *2019 IEEE/CVF Conference on Computer Vision and Pattern Recognition (CVPR)*, 2019, pp. 12 689–12 697.
- [35] S. Shi, X. Wang, and H. Li, "Pointtrnn: 3d object proposal generation and detection from point cloud," in *2019 IEEE/CVF Conference on Computer Vision and Pattern Recognition (CVPR)*, 2019, pp. 770–779.
- [36] T. Yin, X. Zhou, and P. Krähenhühl, "Center-based 3d object detection and tracking," in *2021 IEEE/CVF Conference on Computer Vision and Pattern Recognition (CVPR)*, 2021, pp. 11 779–11 788.
- [37] Z. Zhou, X. Zhao, Y. Wang, P. Wang, and H. Foroosh, "Centerformer: Center-based transformer for 3d object detection," in *Computer Vision – ECCV 2022*, S. Avidan, G. Brostow, M. Cissé, G. M. Farinella, and T. Hassner, Eds. Cham: Springer Nature Switzerland, 2022, pp. 496–513.
- [38] H. Wang, C. Shi, S. Shi, M. Lei, S. Wang, D. He, B. Schiele, and L. Wang, "Dsvt: Dynamic sparse voxel transformer with rotated sets," in *Proceedings of the IEEE/CVF Conference on Computer Vision and Pattern Recognition (CVPR)*, June 2023, pp. 13 520–13 529.
- [39] X. Pan, P. Luo, J. Shi, and X. Tang, "Two at once: Enhancing learning and generalization capacities via ibn-net," in *Computer Vision – ECCV 2018*, V. Ferrari, M. Hebert, C. Sminchisescu, and Y. Weiss, Eds. Cham: Springer International Publishing, 2018, pp. 484–500.
- [40] R. Théodose, D. Denis, T. Chateau, V. Fremont, and P. Checchin, "A deep learning approach for lidar resolution-agnostic object detection," *IEEE Transactions on Intelligent Transportation Systems*, vol. 23, no. 9, pp. 14 582–14 593, 2022.

- [41] A. Torralba and A. A. Efros, "Unbiased look at dataset bias," in *IEEE Conference on Computer Vision and Pattern Recognition (CVPR)*, 2011, pp. 1521–1528.

### A. Parameter set for LSS

Studied models for LSS, SalsaNext, PolarSeg, KPConv, Helix4D, Cylinder3D, SRUNet, and SPVCNN, were taken from their respective official github and trained with the standard hyperparameters shared by the authors.

For IBN-Net, we apply instance normalization at the same position as [3].

For PolarMix, we use the official repository, and apply scene mixing with a probability of 0.5 and object mixing with a probability of 0.5.

The LSS annotation is guaranteed between 5 and 50m away from the sensor, and as such, the mIoU is computed within this range.

### B. Parameter set for LOD

Studied models for LOD, SECOND, PointRCNN, PointPillars, PV-RCNN, and CenterPoint, were taken from the framework OpenPCDet<sup>4</sup> and trained with the standard hyperparameters for 30 epochs.

For IBN-Net, we apply an instance normalization layer to both the 3D backbone of PV-RCNN as well as its compressed 2D Bird's Eye View (BEV) map of features. For the 3D backbone, instance normalization is applied after the first, second to last and last convolutional blocks, before the ReLU activation layer. For the 2D BEV map, instance normalization is also applied in that same order.

In the case of RayDrop, we drop between 25 and 60 percent of LiDAR beams to emulate lower-resolution sensors, similarly to Theodose et al. [40].

All predictions at transfer time are filtered according to a maximum range of 50 m, predictions at the same location are also filtered using a NMS algorithm with a 0.1 IoU threshold. As previously mentioned, we also filter ground truth bounding box during evaluation to only keep boxes with strictly more than 5 points contained within them.

### C. LSS labels

Examples for all 42 labels of LiDAR Semantic Segmentation of our dataset ParisLuco3D are shown in Figure 6 and Figure 7.

### D. LOD labels

Examples for all 11 labels of LiDAR Object Detection and Tracking of our dataset ParisLuco3D are shown in Figure 8.

### E. Label mapping for LSS

1) *SemanticKITTI to ParisLuco3D*: We use the following mapping for the SemanticKITTI dataset to our ParisLuco3D labels, unmentioned labels are discarded:

- Car  $\rightarrow$  car
- Bicycle, Bicyclist  $\rightarrow$  bicycle, scooter
- Bicyclist  $\rightarrow$  bicyclist
- Motorcycle  $\rightarrow$  motorcycle

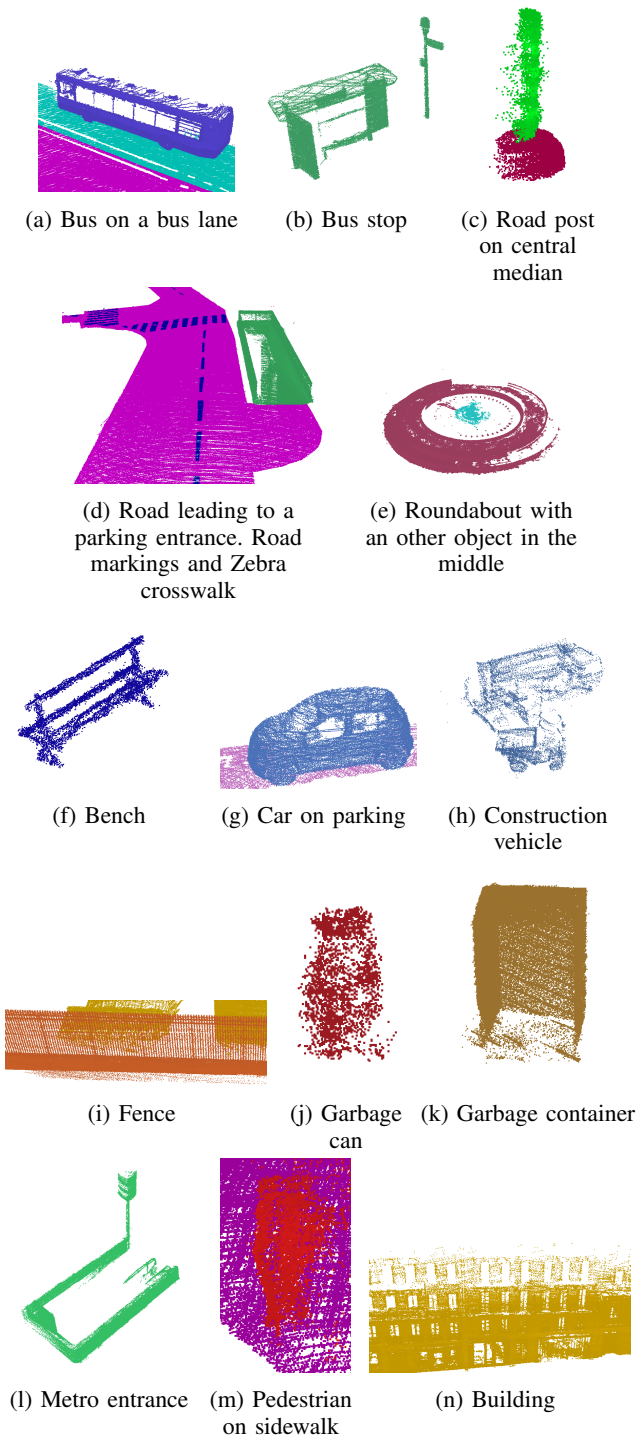


Fig. 6: Labels for LSS.

<sup>4</sup><https://github.com/open-mmlab/OpenPCDet>

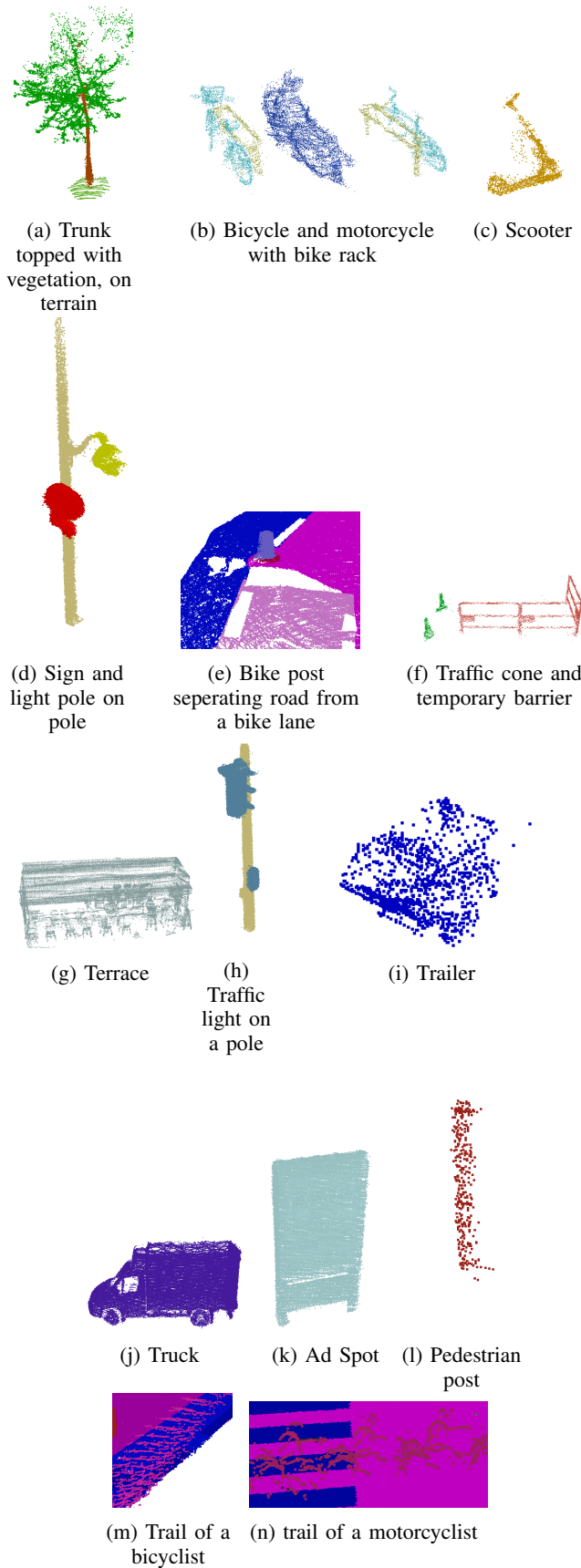


Fig. 7: Labels for LSS.

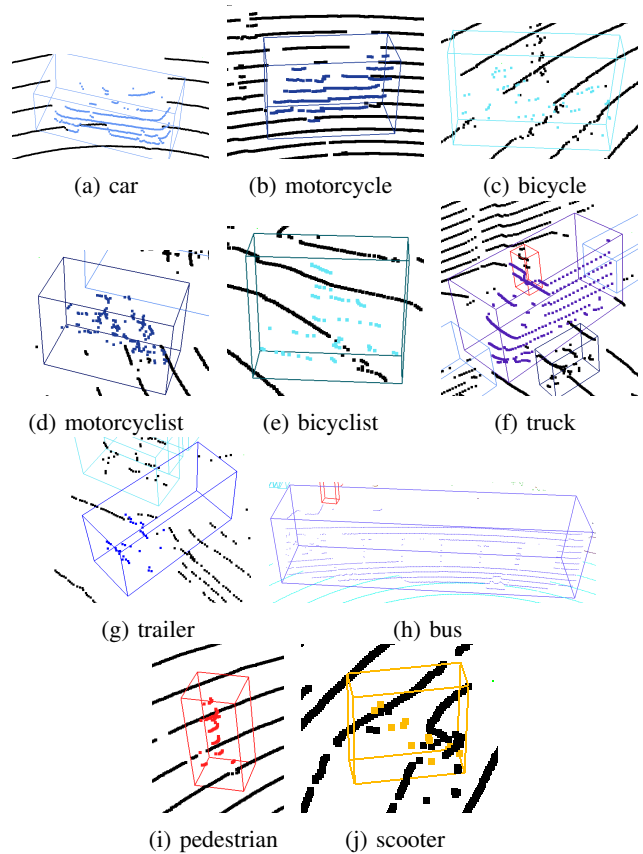


Fig. 8: Labels for LOD. While scootercyclist was annotated, none were found in the dataset.

- Motorcyclist → motorcyclist
- Truck → truck
- Other-vehicle → bus, trailer
- Person → pedestrian
- Road → road, bike lane, bus lane, road markings, zebra crosswalk
- Parking → parking
- Sidewalk → sidewalk
- Other-ground → roundabout, central median
- Building → building
- Fence → fence, temporary barrier
- Vegetation → vegetation
- Trunk → trunk
- Terrain → terrain
- Pole → pole
- Traffic-sign → road sign, traffic light, light pole

2) *nuScenes to ParisLuco3D*: We use the following mapping for the nuScenes dataset to our ParisLuco3D labels, unmentioned labels are discarded:

- barrier → temporary barrier
- bicycle → bicycle, scooter
- bus → bus
- car → car
- construction-vehicle → construction vehicle
- motorcycle → motorcycle
- pedestrian → pedestrian

- traffic-cone → traffic-cone
- trailer → trailer
- truck → truck
- driveable-ground → road, road markings, zebra crosswalk, bus lane, parking
- other-flat → central median, roundabout
- sidewalk → sidewalk, bike lane
- terrain → terrain
- manmade → road post, pedestrian post, ad spot, restaurant terrace, metro entrance, parking entrance, bike post, road sign, bus stop, fence, garbage can, garbage container, bench, building, pole, bike rack, traffic light, light pole
- vegetation → trunk, vegetation

#### F. Label mapping for LOD

1) *nuScenes to ParisLuco3D*: We use the following mapping for the nuScenes dataset to our ParisLuco3D labels:

- car → car
- bus → bus
- truck → truck
- trailer → trailer
- bicycle → bicycle, bicyclist
- motorcycle → motorcycle, motorcyclist
- pedestrian → pedestrian

2) *ONCE to ParisLuco3D*: We use the following mapping for the ONCE dataset to our ParisLuco3D labels:

- Car → car
- Bus → bus
- Truck → truck
- Cyclist → bicycle, bicyclist, motorcycle, motorcyclist
- Pedestrian → pedestrian

3) *Waymo to ParisLuco3D*: We use the following mapping for the Waymo dataset to our ParisLuco3D labels:

- Vehicle → car, bus, truck, trailer, motorcycle, motorcyclist
- Cyclist → bicycle, bicyclist
- Pedestrian → pedestrian

Five scans are released with ground truth semantic labels and ground-truth object detection for qualitative comparisons of future methods (shown in Figure 9).

Quantitative results of our benchmark are in Table VIII, Table IX, Table XI, and Table X.

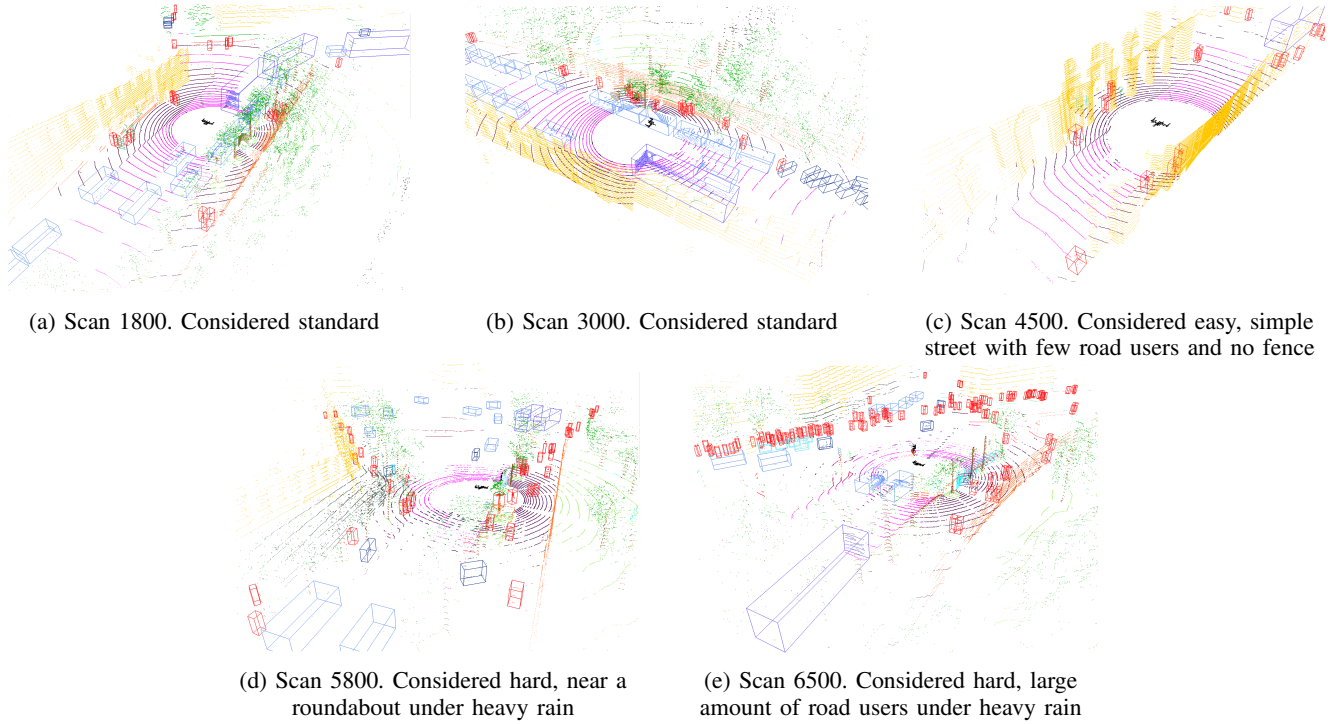


Fig. 9: The 5 scans released for qualitative evaluation.

	Car	Bicycle	Motorcycle	Truck	Other-vehicle	Person	Bicyclist	Motorcyclist	Road	Parking	Sidewalk	Other-ground	Building	Fence	Vegetation	Trunk	Terrain	Pole	Traffic-sign	mIoU	mIoU <sub>SK</sub>
CENet	27.1	0.0	0.3	1.2	19.9	5.8	2.5	2.2	64.3	2.3	56.2	2.8	64.9	2333	44.0	28.1	6.9	35.0	24.5	21.6	58.8
PolarSeg	0.4	0.0	0.0	0.0	7.1	0.0	0.0	0.0	31.2	0.7	24.7	0.4	46.4	21.9	22.4	6.0	11.3	8.8	1.0	9.6	61.8
KPConv	39.7	5.8	8.9	0.3	5.1	30.8	8.8	0.3	8.1	0.6	41.5	0.7	58.6	11.7	67.0	49.9	14.1	26.8	7.1	20.3	61.8
SRUNet	70.5	0.3	12.4	4.7	32.1	20.6	22.6	1.3	71.5	0.1	66.8	0.1	67.3	18.0	71.5	44.9	15.8	41.8	19.3	30.7	63.2
SPVCNN	67.5	0.4	12.3	4.5	18.9	21.9	17.2	0.0	66.7	0.2	67.2	0.1	66.3	12.0	71.7	44.2	11.0	39.5	27.2	28.9	63.4
Helix4D	15.8	0.5	0.0	0.1	4.7	3.0	2.3	0.4	55.1	2.7	42.8	2.1	40.5	22.2	51.1	27.4	7.7	28.8	38.1	18.3	63.9
Cylinder3D	47.1	2.7	2.5	0.3	15.2	11.5	6.8	0.0	58.9	3.9	57.3	1.7	65.9	36.7	54.7	24.8	10.8	32.6	3.6	23.0	64.9

TABLE VIII: Generalization baseline when trained on SemanticKITTI and evaluated on ParisLuco3D. mIoU<sub>SK</sub> denotes the result on the validation split of SemanticKITTI.

	barrier	bicycle	bus	car	cnstrcn-vhel	motorcycle	pedestrian	traffic-cone	trailer	truck	drvbl-grnd	other-flat	sidewalk	terrain	manmade	vegetation	mIoU	mIoU <sub>NS</sub>
CENet	4.1	4.7	35.7	61.6	1.6	22.7	51.6	0	0	6.1	77.4	22.5	56.7	13.3	81.1	66.6	31.6	69.1
PolarSeg	2.1	0.3	1.4	3.2	0.5	1.1	7.0	0	0	0.8	28.7	0.4	20.5	14.0	50.9	49.5	11.3	71.4
KPConv	2.6	0.3	15.9	39.8	0.3	12.0	44.5	0.2	0	2.0	56.2	0.1	17.5	11.7	82.8	79.8	22.9	64.2
SRUNet	4.1	6.4	61.6	82.6	6.5	35.2	60.9	1.2	0	18.8	68.6	7.8	51.2	22.6	87.7	83.6	37.4	69.3
SPVCNN	6.5	4.5	64.5	80.5	4.1	36.2	63.2	0.9	0	15.0	71.1	16.5	61.7	22.8	89.2	82.7	38.7	66.8
Helix4D	1.0	0.4	9.2	29.2	0.1	2.4	9.3	0	0	0.1	57.4	5.8	40.8	13.0	71.5	65.3	19.2	69.3
Cylinder3D	0.1	0.1	51.9	65.6	1.0	18.8	3.2	1.7	0	9.3	71.	8.4	61.3	1.6	74.4	38.8	25.5	74.8

TABLE IX: Generalization baseline when trained on nuScenes and evaluated on ParisLuco3D. mIoU<sub>NS</sub> denotes the result on the validation split of nuScenes.

	car	bus	truck	trailer	bicycle	bicyclist	motorcycle	motorcyclist	scooter	scootercyclist	pedestrian	mAP	mAP <sub>ON</sub>
PointRCNN	12.6	5.3	5.2	-			2.8		-	-	15.7	8.3	28.6
PointPillars	2.6	4.4	1.6	-			1.1		-	-	52.3	12.4	45.5
PV-RCNN	6.5	7.8	3.2	-			2.1		-	-	33.6	10.6	52.4
SECOND	5.3	6.5	1.6	-			1.9		-	-	34.1	9.9	54.0
CenterPoint	4.3	4.1	1.8	-			1.7		-	-	30.6	8.5	59.5
PV-RCNN +RayDrop	14.9	9.7	5.2	-			2.9		-	-	53.0	17.1	48.3
PV-RCNN +IBN-Net	15.6	10.4	6.3	-			3.5		-	-	49.3	17.0	47.0

TABLE X: Generalization baseline for 3D Object Detection when trained on ONCE and evaluated on ParisLuco3D.

	car	bus	truck	trailer	bicycle	bicyclist	motorcycle	motorcyclist	scooter	scootercyclist	pedestrian	mAP	mAP <sub>w</sub>
PointRCNN		27.7		-			3.2		-	-	17.7	16.2	47.9
PointPillars		26.3		-			2.5		-	-	61.9	30.2	68.1
PV-RCNN		30.6		-			2.0		-	-	35.9	22.8	72.3
SECOND		29.7		-			1.3		-	-	38.1	23.0	69.5
CenterPoint		27.2		-			2.3		-	-	46.3	25.3	77.6

TABLE XI: Generalization baseline for 3D Object Detection when trained on Waymo and evaluated on ParisLuco3D.